

MOD-Net: A Machine Learning Approach via Model-Operator-Data Network for Solving PDEs

Lulu Zhang¹, Tao Luo^{1,2}, Yaoyu Zhang^{1,2,3}, Zhi-Qin John Xu^{1,2,*},
Zheng Ma^{1,2,*}

¹ School of Mathematical Sciences, Institute of Natural Sciences, Shanghai Jiao Tong University, Shanghai, 200240, China.

² MOE-LSC and Qing Yuan Research Institute, Shanghai Jiao Tong University, Shanghai, 200240, China.

³ Shanghai Center for Brain Science and Brain-Inspired Technology, Shanghai, 200031, China

Abstract. In this paper, we propose a model-operator-data network (MOD-Net) for solving PDEs. A MOD-Net is driven by a model to solve PDEs based on operator representation with regularization from data. In this work, we use a deep neural network to parameterize the Green's function. The empirical risk consists of the mean square of the governing equation, boundary conditions, and a few labels, which are numerically computed by traditional schemes on coarse grid points with cheap computation cost. With only the labeled dataset or only the model constraints, it is insufficient to accurately train a MOD-Net for complicate problems. Intuitively, the labeled dataset works as a regularization in addition to the model constraints. The MOD-Net is much efficient than original neural operator because the MOD-Net also uses the information of governing equation and the boundary conditions of the PDE rather than purely the expensive labels. Since the MOD-Net learns the Green's function of a PDE, it solves a type of PDEs but not a specific case. We numerically show MOD-Net is very efficient in solving Poisson equation and one-dimensional Boltzmann equation. For non-linear PDEs, where the concept of the Green's function does not apply, the non-linear MOD-Net can be similarly used as an ansatz for solving non-linear PDEs.

1 Introduction

Using deep neural network (DNN) in solving PDEs attracts more and more attention [3, 4, 6, 7, 10, 12–14, 16, 17]. We review three DNN approaches for solving PDEs.

The first approach is to parameterize the solution by a DNN and the empirical risk can be the mean square of the residual of differential equation [16] or in variational forms [4, 13],

*Corresponding author. Email addresses: zhang19661@sjtu.edu.cn (Z. Zhang), luotao41@sjtu.edu.cn (T. Luo), zhyy.sjtu@sjtu.edu.cn (Y. Zhang), xuzhiqin@sjtu.edu.cn (Z. Xu), zhengma@sjtu.edu.cn (Z. Ma)

by minimizing which the function learned by the DNN can satisfy the differential equation. This parameterization approach can solve very high-dimensional PDEs and does not require any labels, however, it only solves a specific PDE in each training trial, that is, once the PDE is changed, such as the source term or the boundary conditions, we have to train a new DNN. An important characteristic of the parameterization approach is indicated by the frequency principle that high frequency is learned very slowly [15, 20, 21]. To overcome the curse of high frequency, a series of multiscale approaches are proposed [1, 10, 14, 18, 19]. The second approach uses DNN to learn the mapping from the source term to the solution [5]. In this mapping approach, the source function and the solution are sampled at fixed positions, that is, two vectors. The vector of the source function is fed into the DNN to predict the vector of the solution function. The advantage of this mapping approach is that the DNN solves the PDE for any source function, thus, it can be much convenient in application. However, the mapping approach can only evaluate the solution at fixed positions and requires large samples, which is often computational inefficient or intractable, especially for high-dimensional PDEs or complicated PDEs, such as radiative transfer equation. The third approach is called neural operator [11, 12], which represents the solution based on the form similar to the idea of the Green's function and the DNN is used to learn the Green's function. The neural operator solves a type of PDEs but not a specific PDE and can be evaluated at any position. The training of the neural operator is to minimize the difference between the learned solution and the true solution at randomly sampled positions. Therefore, the neural operator is a data-driven method and requires a large amount of labels, a similar difficulty to the mapping approach.

In this work, we propose a machine learning approach via model-operator-data network (MOD-Net) for Solving PDEs. The MOD-Net has advantages including: i) evaluating the solution at whole space; ii) requiring none or a few labels numerically computed by traditional scheme on coarse grid points with cheap computation; iii) solving a type of PDEs but not a specific PDE. The three key components of MOD-Net are illustrated as follows.

Model driven. MOD-Net is driven by the physical model to avoid using expensive labeled data. That is, the empirical risk, i.e., training loss requires the solution satisfying the constraints of the governing PDE and boundary conditions. To realize the model constraint, one can use various methods, such as minimizing the mean square of the residual of the governing PDE and boundary conditions (e.g., physics-informed neural network [16]), or minimizing the variational form of the governing PDE and boundary conditions (e.g., Deep-Ritz method [4]).

Operator representation. Similar to the neural operator [11, 12], the MOD-Net represents the solution operator of a PDE, i.e, mapping between source terms, boundary conditions, or parameters and the solution, based on the the equation/model. In this work DNN is used to parameterize the Green's function, however, it is not restricted to use Green's function and can be generalized to other architectures. This operator representation utilizes the invariant characteristic of Green's function in solving PDE, thus, might be more efficient than an end-to-end representation by parameterizing solution with a DNN

directly.

Data regularization In MOD-Net, we find that in complicate problems, with only the model constraints, the solution is often not accurate enough even when the empirical risk is reasonably small. To overcome this problem, we add a regularization term by minimizing the difference between the MOD-Net prediction and a few labels numerically computed by traditional scheme on coarse grid points with cheap computation cost. Note that with only the small amount of labeled data, the MOD-Net cannot be well trained either. Therefore, the effect of the labeled data in MOD-Net is different from supervised learning, in which a DNN training often requires a large amount of accurate labeled data. Intuitively, the effect of data in MOD-Net works as an regularization similar to various regularization terms in traditional optimization problems.

We first apply MOD-Net to solving simple Poisson equations, in which we show that without labels, MOD-Net with the mean square of PDE, i.e., governing equation and boundary conditions, can learn the Poisson equation well. We further apply MOD-Net to the radiative transfer equation [2, 9], which is important in many applications, such as neutron transport, radiative transfer and quantum mechanics. However, the computational cost of solving the radiative transfer equation with traditional schemes is very high. Many numerical schemes are devoted to efficiently solving the radiative transfer equation [8]. In this work, with the mean square of PDE, i.e., governing equation and boundary conditions, we can well train MOD-Net with a few cheap labels for radiative transfer equation with flexible boundary conditions. In real applications, the boundary conditions of the radiative transfer equation vary frequently. For example, the radiation entering and leaving the medium varies in different experimental trials and can be measured, a well trained MOD-Net can infer the density distribution over the medium fast. Therefore, an important advantage is that a well-trained MOD-Net can very efficiently infer the solution for given boundary conditions.

The rest of the paper is organized as follows. In section 2, we will introduce DNNs. Section 3 will present MOD-Net structures. Section 4 will show the numerical results for Poisson equations. In section 5, we show numerical experiments for one-dimensional radiative transfer equation. Finally, section 6 gives a conclusion and some discussions for further work.

2 Preliminary: Deep neural networks

We introduce the following conventional notations for DNNs[‡]. An L -layer neural network is defined recursively as,

$$f_{\theta}^{[0]}(\mathbf{x}) = \mathbf{x}, \quad (2.1)$$

$$f_{\theta}^{[l]}(\mathbf{x}) = \sigma \circ (W^{[l-1]} f_{\theta}^{[l-1]}(\mathbf{x}) + \mathbf{b}^{[l-1]}), \quad 1 \leq l \leq L-1, \quad (2.2)$$

$$f_{\theta}(\mathbf{x}) = f_{\theta}^{[L]}(\mathbf{x}) = W^{[L-1]} f_{\theta}^{[L-1]}(\mathbf{x}) + \mathbf{b}^{[L-1]}, \quad (2.3)$$

where $W^{[l]} \in \mathbb{R}^{m_{l+1} \times m_l}$, $\mathbf{b}^{[l]} \in \mathbb{R}^{m_{l+1}}$, $m_0 = d_{\text{in}} = d$ is the input dimension, $m_L = d_{\text{out}}$ is the output dimension, σ is a scalar function and “ \circ ” means entry-wise operation. We denote the set of parameters by θ .

A loss function $\ell(f_{\theta}(\mathbf{x}), \mathbf{y})$ measures the difference between a predicted label and a true label. The empirical risk, also known as the training loss, for a set $S = \{(\mathbf{x}_i, \mathbf{y}_i)\}_{i=1}^n$ is denoted by $R_S(\theta)$,

$$R_S(\theta) = \frac{1}{n} \sum_{i=1}^n \ell(f_{\theta}(\mathbf{x}_i), \mathbf{y}_i). \quad (2.4)$$

More generally, the empirical risk can be defined without labels. For example, if we want to learn the solution $f(\mathbf{x})$ of an equation, i.e., $\mathcal{L}[f](\mathbf{x}) = \mathbf{0}$ for $\mathbf{x} \in \Omega$, the empirical risk for this equation can be defined by

$$R_S(\theta) = \frac{1}{n} \sum_{i=1}^n \|\mathcal{L}[f_{\theta}](\mathbf{x}_i)\|_2^2, \quad (2.5)$$

where the data set S is randomly sampled from Ω during each iteration step. The empirical risk can be also defined by the weighted summation of the empirical risk of the labeled data and the empirical risk of the equation. If more requirements exist in the problem, such as boundary conditions, the empirical risk can be similarly defined. Two common empirical risks for solving PDEs are calculated with least square loss (e.g., physics-informed neural network [16]) and variational loss (e.g., Deep-Ritz method [4]).

3 Model-operator-data network (MOD-Net)

Our goal is to solve the following PDE fast and accurately,

$$\begin{cases} \mathcal{L}_{\sigma}[u](\mathbf{x}) = g(\mathbf{x}), & \mathbf{x} \in \Omega, \\ u(\mathbf{x}) = \phi(\mathbf{x}), & \mathbf{x} \in \partial\Omega, \end{cases} \quad (3.1)$$

[‡]BAAI.2020. Suggested Notation for Machine Learning. <https://github.com/mazhengcn/suggested-notation-for-machine-learning>.

where \mathcal{L} is a linear operator and σ involves terms which determine the governing equation of PDE, e.g., the absorption coefficients in the radiative transfer equation.

Our basic idea is to use a DNN to learn the operator $\mathcal{G} : (\phi, \sigma, g) \mapsto u$, i.e., for each given boundary condition, ϕ , control term σ and source term g , there is $\mathcal{G}(\phi, \sigma, g) = u$.

For a linear PDE, Green's function can help us obtain the solution of PDE due to the superposition principle. With the Green's function method, we have the following formal representation of the solution of PDE (3.1),

$$u(\mathbf{x}; \phi, \sigma, g) = \int_{\Omega} G_1(\mathbf{x}, \mathbf{x}'; \sigma) g(\mathbf{x}') d\mathbf{x}' + \int_{\partial\Omega} G_2(\mathbf{x}, \mathbf{x}'; \sigma) \phi(\mathbf{x}') d\mathbf{x}'. \quad (3.2)$$

where for any fixed $\mathbf{x}' \in \Omega$, $G_1(\mathbf{x}, \mathbf{x}'; \sigma)$ is the solution of the following PDE,

$$\begin{cases} \mathcal{L}_\sigma[G_1](\mathbf{x}) = \delta(\mathbf{x} - \mathbf{x}'), & \mathbf{x} \in \Omega, \\ G_1(\mathbf{x}, \mathbf{x}'; \sigma) = 0, & \mathbf{x} \in \partial\Omega, \end{cases}$$

and for any fixed $\mathbf{x}' \in \partial\Omega$, $G_2(\mathbf{x}, \mathbf{x}'; \sigma)$ is the solution of the following PDE,

$$\begin{cases} \mathcal{L}_\sigma[G_2](\mathbf{x}) = 0, & \mathbf{x} \in \Omega, \\ G_2(\mathbf{x}, \mathbf{x}'; \sigma) = \delta(\mathbf{x} - \mathbf{x}'), & \mathbf{x} \in \partial\Omega. \end{cases}$$

However, it is difficult to obtain the analytical formula of the Green's functions. In the following, we consider using DNN to represent operators G_1 and G_2 . Since G_1 and G_2 are similar, we use G_1 as an example for illustration. G_1 is an operator that is imposed on function $\sigma(\mathbf{x})$ to derive another function $G_1(\mathbf{x}, \mathbf{x}'; \sigma)$. Generally, it is not possible to design a DNN taking functions as input. In this work, we consider function $\sigma(\mathbf{x})$ that can be parameterized by a vector \mathbf{p}_σ . For example, $\sigma(\mathbf{x}) = a\mathbf{x} + b$ can be parameterized by $\mathbf{p}_\sigma = (a, b)$. Then, a DNN $f_{\theta_1}(\mathbf{x}, \mathbf{x}', \mathbf{p}_\sigma)$ is trained to represent $G_1(\mathbf{x}, \mathbf{x}'; \sigma)$, similarly, another DNN $f_{\theta_2}(\mathbf{x}, \mathbf{x}', \mathbf{p}_\sigma)$ is for $G_2(\mathbf{x}, \mathbf{x}'; \sigma)$. By implementing $f_{\theta_1}(\mathbf{x}, \mathbf{x}', \mathbf{p}_\sigma)$ and $f_{\theta_2}(\mathbf{x}, \mathbf{x}', \mathbf{p}_\sigma)$ into Eq. (3.2), we obtain a representation $u_{\theta_1, \theta_2}(\mathbf{x}; \phi, \sigma, g)$ for $u(\mathbf{x}; \phi, \sigma, g)$. In application, the integration in Eq. (3.2) is realized by discrete numerical schemes. For example, we consider Monte-Carlo algorithm. We uniformly sample a set $S_{G, \Omega}$ from Ω and a set $S_{G, \partial\Omega}$ from $\partial\Omega$, then,

$$u_{\theta_1, \theta_2}(\mathbf{x}; \phi, \sigma, g) = \frac{|\Omega|}{|S_{G, \Omega}|} \sum_{\mathbf{x}' \in S_{G, \Omega}} f_{\theta_1}(\mathbf{x}, \mathbf{x}', \mathbf{p}_\sigma) g(\mathbf{x}') + \frac{|\partial\Omega|}{|S_{G, \partial\Omega}|} \sum_{\mathbf{x}' \in S_{G, \partial\Omega}} f_{\theta_2}(\mathbf{x}, \mathbf{x}', \mathbf{p}_\sigma) \phi(\mathbf{x}'). \quad (3.3)$$

To train the neural networks, we would utilize the information of PDE, i.e., governing equation and boundary condition, and a fewdata $S^{u, k} = \{\mathbf{x}_i, u^k(\mathbf{x}_i)\}_{i \in [n_k]}$ for each $\{\phi^k, \sigma^k, g^k\}, k = 1, 2, \dots, K$, where $u^k(\cdot) = u(\cdot; \phi^k, \sigma^k, g^k)$. Note that $S^{u, k}$ can be numerically solved by traditional schemes on coarse grid points, which is not computationally expensive. To utilize the constraint of governing equation of PDE, for each k , we uniformly sample a set of data from Ω , i.e., $S^{\Omega, k}$. To utilize the information of boundary constraint,

for each k , we uniformly sample a set of data from $\partial\Omega$, i.e., $S^{\partial\Omega,k}$. Then, we train the neural networks by minimizing the empirical risk, whose definition is as follows,

$$\begin{aligned} R_S = & \frac{1}{K} \sum_{k \in [K]} \left(\lambda_1 \frac{1}{|S^{\Omega,k}|} \sum_{\mathbf{x} \in S^{\Omega,k}} \|\mathcal{L}_{\sigma^k} [u_{\theta_1, \theta_2}(\mathbf{x}; \phi^k, \sigma^k, g^k)](\mathbf{x}) - g^k(\mathbf{x})\|_2^2 \right. \\ & + \lambda_2 \frac{1}{|S^{\partial\Omega,k}|} \sum_{\mathbf{x} \in S^{\partial\Omega,k}} \|u_{\theta_1, \theta_2}(\mathbf{x}; \phi^k, \sigma^k, g^k) - \phi^k(\mathbf{x})\|_2^2 \\ & \left. + \lambda_3 \frac{1}{n_k} \sum_{i \in [n_k]} \|u_{\theta_1, \theta_2}(\mathbf{x}_i; \phi^k, \sigma^k, g^k) - u^k(\mathbf{x}_i)\|_2^2 \right), \end{aligned} \quad (3.4)$$

where $\lambda_1, \lambda_2, \lambda_3$ are hyperparameters used to tune the importance of each part in the total risk. An important advantage of our proposed MOD-Net method is that we take advantage of the PDE constraint and use cheap not-so-accurate labeled data.

In real applications, depending on the problems, if the boundary condition is zero, such as the Poisson case in section 4, G_2 is ignored, and if the source term is zero, such as the Boltzmann case in section 5, G_1 is ignored. For one-dimensional case, the integration over boundary is the summation at two points, therefore, we can use two DNNs to learn $G_2(\mathbf{x}, \mathbf{x}'; \sigma)|_{\mathbf{x}'=\mathbf{x}_L}$ and $G_2(\mathbf{x}, \mathbf{x}'; \sigma)|_{\mathbf{x}'=\mathbf{x}_R}$, respectively, where \mathbf{x}_L and \mathbf{x}_R are boundary points. The input of the two DNNs are lower dimensional due to the fixation of \mathbf{x}' . The amount of the labeled data required also depends on the problem. For simple problems, such as Poisson problem, we use no labeled data, but for Boltzmann problem with complicate coefficients, we use a few labeled data.

4 Numerical experiments: 2D Poisson equation

We consider the Poisson equation,

$$\begin{aligned} -\Delta u(\mathbf{x}) &= g(\mathbf{x}), \quad \mathbf{x} \in \Omega, \\ u(\mathbf{x}) &= 0, \quad \mathbf{x} \in \partial\Omega. \end{aligned} \quad (4.1)$$

Consider 2D case, in which source function $g(x, y) = -a(x^2 - x + y^2 - y)$, i.e.,

$$\begin{aligned} \partial_{xx}u + \partial_{yy}u &= a(x^2 - x + y^2 - y), \quad (x, y) \in \Omega, \\ u &= 0, \quad (x, y) \in \partial\Omega, \end{aligned} \quad (4.2)$$

where $\Omega = [0, 1]^2$ and a controls the source term. Obviously, the analytical solution is $u(x, y; g) = \frac{a}{2}x(x-1)y(y-1)$.

4.1 Use DNN to fit Green's function

Using the Green's function method, the solution of (4.1) can be represented by

$$u(\mathbf{x}; g) = \int_{\Omega} G(\mathbf{x}, \mathbf{x}') g(\mathbf{x}') d\mathbf{x}', \quad (4.3)$$

where for any $x' \in \Omega$, the Green's function $G(x, x')$ is the solution of following problem,

$$\begin{aligned} -\Delta G(x, x') &= \delta(x - x') \quad x \in \Omega \\ G(x, x') &= 0, \quad x \in \partial\Omega. \end{aligned} \quad (4.4)$$

In the considered 2D case, $g(x, y) = -a(x^2 - x + y^2 - y)$, we have

$$u(x, y; g) = \int_0^1 \int_0^1 G(x, y, x', y') g(x', y') dx' dy'. \quad (4.5)$$

For demonstration, although we can obtain the analytical form of the Green's function, we use a deep neural network of hidden layer size 128-128-128-128 $f_\theta(x, y, x', y')$ to fit the green's function $G(x, y, x', y')$ instead.

When we calculate the integral, it is impossible to integrate it analytically. In practical, we often use the numerical integration. We use the Gauss-Legendre integral. Then we can represent neural operator $u_\theta(x, y; g)$ with green's function DNN $f_\theta(x, y, x', y')$, that is,

$$u_\theta(x, y; g) = \sum_{x' \in S_{G_x}} \sum_{y' \in S_{G_y}} \omega_{x'} \omega_{y'} f_\theta(x, y, x', y') g(x', y'), \quad (4.6)$$

where $S_{G_x} \subset [0, 1]$, $S_{G_y} \subset [0, 1]$ consist fixed integration points, determined by 1D Gauss-Legendre integral method and $\omega_{x'}$, $\omega_{y'}$ are corresponding coefficients.

4.2 Empirical risk function

For this toy example, to train the neural networks, we use no labeled data and only utilize the information of PDE, i.e., governing equation and boundary condition, for each $g^k, k = 1, 2, \dots, K$. To utilize the constraint of governing equation of PDE, we uniformly sample a set of data from $\Omega = [0, 1] \times [0, 1]$, i.e., $S^{\Omega, k}$. To utilize the information of boundary constraint, for each k , we uniformly sample a set of data from $\partial\Omega$. Since the boundary $\partial\Omega$ consists of four line segments, i.e., $\partial\Omega = \bigcup_{i=1}^4 \partial\Omega_i$, where $\partial\Omega_1 = \{(0, y)\}_{y \in [0, 1]}, \partial\Omega_2 = \{(1, y)\}_{y \in [0, 1]}, \partial\Omega_3 = \{(x, 0)\}_{x \in [0, 1]}, \partial\Omega_4 = \{(x, 1)\}_{x \in [0, 1]}$, we uniformly sample a set of data from $\partial\Omega_i$ respectively, i.e., $S^{\partial\Omega_i, k}$, $i = 1, 2, 3, 4$.

Since we use no labeled data, λ_3 in the general definition (3.4) is set as zero. The

empirical risk for this example is as follows,

$$\begin{aligned}
R_S = & \frac{1}{K} \sum_{k \in [K]} \left(\lambda_1 \frac{1}{|S^{\Omega,k}|} \sum_{(x,y) \in S^{\Omega,k}} \left(-(\partial_{xx} u_{\theta}(x,y;g^k) + \partial_{yy} u_{\theta}(x,y;g^k)) - g^k(x,y) \right)^2 \right. \\
& + \lambda_2 \frac{1}{|S^{\partial\Omega_1,k}|} \sum_{(x,y) \in S^{\partial\Omega_1,k}} u_{\theta}(x,y;g^k)^2 \\
& + \lambda_2 \frac{1}{|S^{\partial\Omega_2,k}|} \sum_{(x,y) \in S^{\partial\Omega_2,k}} u_{\theta}(x,y;g^k)^2 \\
& + \lambda_2 \frac{1}{|S^{\partial\Omega_3,k}|} \sum_{(x,y) \in S^{\partial\Omega_3,k}} u_{\theta}(x,y;g^k)^2 \\
& \left. + \lambda_2 \frac{1}{|S^{\partial\Omega_4,k}|} \sum_{(x,y) \in S^{\partial\Omega_4,k}} u_{\theta}(x,y;g^k)^2 \right). \tag{4.7}
\end{aligned}$$

Note that, the least square loss in (3.4) is not crucial. To demonstrate it, we also use the variational loss used in Deep Ritz Method and the empirical risk is as follows,

$$\begin{aligned}
R_S = & \frac{1}{K} \sum_{k \in [K]} \left(\lambda_1 \frac{1}{|S^{\Omega,k}|} \sum_{(x,y) \in S^{\Omega,k}} \left(\frac{1}{2} (|\partial_x u_{\theta}(x,y;g^k)|^2 + |\partial_y u_{\theta}(x,y;g^k)|^2) - g^k(x,y) u_{\theta}(x,y;g^k) \right) \right. \\
& + \lambda_2 \frac{1}{|S^{\partial\Omega_1,k}|} \sum_{(x,y) \in S^{\partial\Omega_1,k}} u_{\theta}(x,y;g^k)^2 \\
& + \lambda_2 \frac{1}{|S^{\partial\Omega_2,k}|} \sum_{(x,y) \in S^{\partial\Omega_2,k}} u_{\theta}(x,y;g^k)^2 \\
& + \lambda_2 \frac{1}{|S^{\partial\Omega_3,k}|} \sum_{(x,y) \in S^{\partial\Omega_3,k}} u_{\theta}(x,y;g^k)^2 \\
& \left. + \lambda_2 \frac{1}{|S^{\partial\Omega_4,k}|} \sum_{(x,y) \in S^{\partial\Omega_4,k}} u_{\theta}(x,y;g^k)^2 \right). \tag{4.8}
\end{aligned}$$

4.3 Learning process

For each training epoch, we first randomly choose source functions $\{g^k\}_{k=1}^K$ and calculate their values on fixed integration points (x', y') , where $x' \in S_{G_x}$ and $y' \in S_{G_y}$. Second, we randomly sample data and obtain data set $S^{\Omega,k}, S^{\partial\Omega_i,k}, i=1,2,3,4$. We obtain the data set $D = \{(x, y, x', y', g^k(x', y')) | (x, y) \in S^{\Omega,k} \cup \bigcup_{i=1}^4 S^{\partial\Omega_i,k}, x' \in S_{G_x}, y' \in S_{G_y}\}$. In the following, we feed the data into the neural network $f_{\theta}(x, y, x', y')$ and calculate the total risk (4.7) or (4.8) with neural operator $u_{\theta}(x, y; g)$, see Eq. (4.6). Train neural network f_{θ} with Adam to minimize the total risk, and finally we obtain a well-trained green's function DNN f_{θ} , furthermore, according to Eq. (4.6), we obtain a neural operator $u_{\theta}(x, y; g)$.

4.4 Results

The source function $g(x,y) = -a(x^2 - x + y^2 - y)$ is determined by a . We then denote source function $g(x,y) = -a(x^2 - x + y^2 - y)$ by g_a . To illustrate our approach, we train a neural operator mapping from g to the solution of the Poisson equation (4.2).

4.4.1 Example 1: MOD-Net for a set of Poisson equations using least square loss

For illustration, we would train the MOD-Net by various source functions and test the MOD-Net with several source functions that are not used for training. In this example, we calculate the empirical risk with least square loss.

In training, for each epoch, we choose a set of source functions, for example, we sample $K=10$ source functions g_a from selected region, that is, we sample control parameter a uniformly from $\{10k\}_{k=1}^{20}$. We set the number of integration points $|S_{G_x}|=10$ and $|S_{G_y}|=10$, and for each epoch, we randomly sample 600 points in $[0,1]^2$ and sample 600 points in each line of boundary, respectively. We set $\lambda_1=1, \lambda_2=1$ in the empirical risk using least square loss (4.7).

We test the performance of this well-trained MOD-Net on $a = 15$. For each fixed a , the corresponding exact true solution is $u(x,y) = \frac{a}{2}x(x-1)y(y-1)$. For visualizing the performance of our well-trained MOD-Net, we show the analytic solution and MOD-Net solution on 101×101 isometric grid points by color. To compare these two solutions more intuitively, we calculate the difference of the two solutions at each point and show the error by color, i.e., as the error increases, the color changes from blue to red, in Fig. 1. The root mean square error (RMSE) is $\sim 2 \times 10^{-3}$. We also show the solution obtained by MOD-Net and the corresponding analytical solution on fixed $x=0, 0.5, 1$ for considered test source function. As shown in Fig. 2, the MOD-Net can well predict the analytic solutions.

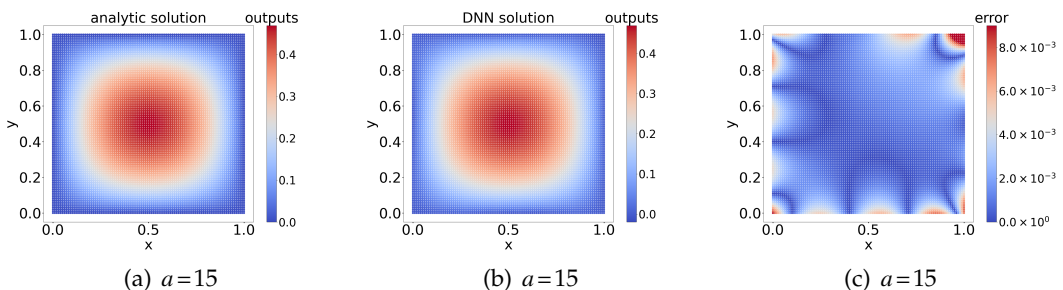


Figure 1: Example 1. Comparison between analytic solution and MOD-Net solution on 101×101 grid points corresponding to source terms determined by $a = 15$. (a) Analytic solution. (b) MOD-Net solution. (c) The difference between the analytic solution and MOD-Net solution. Since the error at most points are very small, here we reduce the upper limit of the Color bar to see more information.

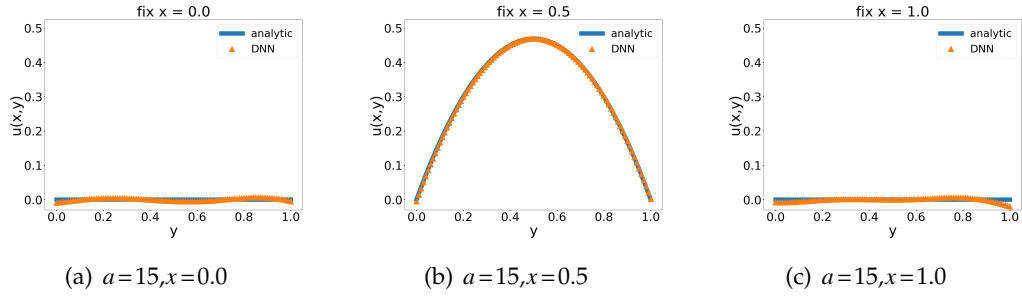


Figure 2: Example 1. Comparison between analytic solution and MOD-Net solution on $x=0, 0.5, 1$ corresponding to source function determined by test $a=15$.

4.4.2 Example 2: MOD-Net for a set of Poisson equations using variational loss

In this experiment, we also train the MOD-Net by various source functions. But, note that, in this example, we calculate the empirical risk with variational loss used in Deep Ritz Method.

In training, for each epoch, similarly we sample control parameter a uniformly from $\{10k\}_{k=1}^{20}$. We set the number of integration points $|S_{G_x}|=10$ and $|S_{G_y}|=10$, and for each epoch, we randomly sample 600 points in $[0,1]^2$ and sample 600 points in each line of boundary, respectively. We set $\lambda_1=1, \lambda_2=100$ in the empirical risk using least square loss (4.8).

We test the performance of this well-trained MOD-Net on $a=15$. For each fixed a , the corresponding exact true solution is $u(x,y)=\frac{a}{2}x(x-1)y(y-1)$. For visualizing the performance of our well-trained MOD-Net, similarly we show the analytic solution and MOD-Net solution on 101×101 isometric grid points by color. To compare these two solutions more intuitively, similarly we calculate the difference of the two solutions at each point and show the error by color in Fig. 3. The root mean square error (RMSE) is $\sim 6\times 10^{-3}$. For visualizing the performance of our well-trained MOD-Net, we show the solution obtained by MOD-Net and the corresponding analytical solution on fixed $x=0, 0.5, 1$ for considered test source function. As shown in Fig. 4, the MOD-Net can well predict the analytic solutions.

5 Numerical experiments: One-dimensional radiative transfer equation

In this section, we would apply MOD-Net to solve one-dimensional radiative transfer equation. Consider the density of particles in a bounded domain that interact with a background through absorption and scattering processes. The density function $u(x,v)$

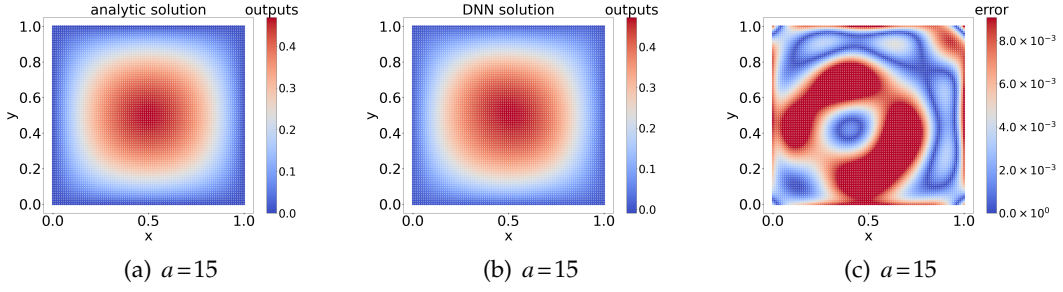


Figure 3: Example 2. Comparison between analytic solution and MOD-Net solution on 101×101 grid points corresponding to source terms determined by $a=15$. (a) Analytic solution. (b) MOD-Net solution. (c) The difference between the analytic solution and MOD-Net solution.

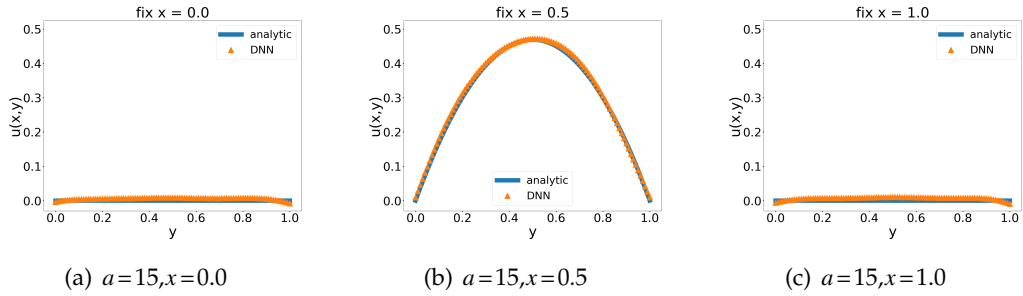


Figure 4: Example 2. Comparison between analytic solution and MOD-Net solution on $x=0,0.5,1$ corresponding to source function determined by test $a=15$.

follows the radiative transfer equation

$$\mathbf{v} \cdot \nabla u(\mathbf{x}, \mathbf{v}) + \frac{\sigma_T(\mathbf{x})}{\varepsilon(\mathbf{x})} u(\mathbf{x}, \mathbf{v}) = \frac{1}{|S|} \left(\frac{\sigma_T(\mathbf{x})}{\varepsilon(\mathbf{x})} - \varepsilon(\mathbf{x}) \sigma_a(\mathbf{x}) \right) \int_S u(\mathbf{x}, \xi) d\xi, \quad (5.1)$$

$$u(\mathbf{x}, \mathbf{v}) = \phi(\mathbf{x}, \mathbf{v}), \quad \mathbf{x} \in \Gamma = \partial \Omega, \quad \mathbf{v} \in S, \quad \mathbf{v} \cdot \mathbf{n}_x < 0,$$

where $\mathbf{x} \in \Omega \subset \mathbb{R}^d$ is the d -dimensional space variable, \mathbf{v} is the angular variable on unit ball $S^{d-1} \subset \mathbb{R}^d$, \mathbf{n}_x is the outward normal vector at \mathbf{x} on the boundary, σ_a is the absorption coefficients, σ_T is the total scattering coefficients and ε is Knudsen number. For simplifying the PDE and well describing the real situation, we use the isotropic hypothesis, then σ_a and σ_T are only related to the space variable \mathbf{x} .

High-accuracy numerical methods are developed to solve radiative transfer equation, e.g., Tailored Finite Point Method (TFPM). However, these numerical methods are usually based on discrete grids. To improve the accuracy, the mesh grid has to be finer and the solving time exponentially increases. Another disadvantage is that these numerical methods usually only solve one particular PDE, i.e., if we change anyone of σ_T , σ_a , ε or

ϕ , we need to reuse this algorithm to solve it. To alleviate these problems, our MOD-Net approach learns the operator $\mathcal{G}:(\phi, \sigma_T, \sigma_a, \varepsilon) \mapsto u$. For convenience, in the following, we denote $\sigma = (\sigma_T, \sigma_a, \varepsilon)$.

We consider one-dimensional radiative transfer equations. Set $\Omega = [x_L, x_R]$, $S = [-1, 1]$, normal vector $n_{x_L} = -1$, $n_{x_R} = 1$, we obtain

$$\begin{aligned} v \partial_x u(x, v) + \frac{\sigma_T(x)}{\varepsilon(x)} u(x, v) &= \left(\frac{\sigma_T(x)}{\varepsilon(x)} - \varepsilon(x) \sigma_a(x) \right) \frac{1}{2} \int_{-1}^1 u(x, \xi) d\xi, \\ u(x_L, v) &= g_L(v), \quad v > 0, \\ u(x_R, v) &= g_R(v), \quad v < 0. \end{aligned} \quad (5.2)$$

Our goal is to train MOD-Net to fit the operator $\mathcal{G}:(g_L, g_R, \sigma) \mapsto u$, where u is the solution of (5.2) with given g_L, g_R, σ .

5.1 Use DNN to fit Green's function

Denote

$$\mathcal{L}_\sigma[u] = v \cdot \nabla u(x, v) + \frac{\sigma_T(x)}{\varepsilon(x)} u(x, v) - \frac{1}{|S|} \left(\frac{\sigma_T(x)}{\varepsilon(x)} - \varepsilon(x) \sigma_a(x) \right) \int_S u(x, \xi) d\xi,$$

the radiative transfer equation (5.1) can be rewritten as the following linear PDE,

$$\begin{cases} \mathcal{L}_\sigma[u](x, v) = 0, & x \in \Omega, \quad v \in S, \\ u(x, v) = \phi(x, v), & x \in \partial\Omega, \quad v \cdot n_x < 0, \end{cases} \quad (5.3)$$

which is a special case of linear PDE (3.1).

Similarly, with Green's function method, the solution of (5.3), can be represented by the following formula,

$$u(x, v; \phi, \sigma) = \int_{\partial\Omega} \int_{S \cap \{v' | v' \cdot n_{x'} < 0\}} G(x, x', v, v'; \sigma) \phi(x', v') d v' d x', \quad (5.4)$$

where $G(x, x', v, v'; \sigma)$ are the solution of the following PDE:

$$\begin{cases} \mathcal{L}_\sigma[G](x, v) = 0, & x \in \Omega, \quad v \in S, \\ G(x, x', v, v') = \delta(v - v') \delta(x - x'), & x, x' \in \partial\Omega, \quad v \cdot n_x < 0, \quad v' \cdot n_{x'} < 0. \end{cases}$$

Since in the one-dimensional example, we consider $\Omega = [x_L, x_R]$, then x' in $G(x, x', v, v'; \sigma)$ only have two choices. We can rewrite the integral in (5.4) by the following formula,

$$u(x, v; g_L, g_R, \sigma) = \int_0^1 G_L(x, v, v'; \sigma) g_L(v') d v' + \int_{-1}^0 G_R(x, v, v'; \sigma) g_R(v') d v', \quad (5.5)$$

where G_L, G_R are the solution of the following two PDEs respectively,

$$\begin{cases} v\partial_x G_L + \frac{\sigma_T}{\varepsilon} G_L = \left(\frac{\sigma_T}{\varepsilon} - \varepsilon\sigma_a\right) \frac{1}{2} \int_{-1}^1 G_L(x, \xi, v'; \sigma) d\xi, \\ G_L(x_L, v, v'; \sigma) = \delta(v - v'), \quad v > 0, \\ G_L(x_R, v, v'; \sigma) = 0, \quad v < 0, \end{cases}$$

$$\begin{cases} v\partial_x G_R + \frac{\sigma_T}{\varepsilon} G_R = \left(\frac{\sigma_T}{\varepsilon} - \varepsilon\sigma_a\right) \frac{1}{2} \int_{-1}^1 G_R(x, \xi, v'; \sigma) d\xi, \\ G_R(x_L, v, v'; \sigma) = 0, \quad v > 0, \\ G_R(x_R, v, v'; \sigma) = \delta(v - v'), \quad v < 0. \end{cases}$$

With the help of green's function method, to achieve our goal of fitting the operator $\mathcal{G} : (g_L, g_R, \sigma) \mapsto u$, where u is the solution of (5.2) with given g_L, g_R, σ , we only need to obtain operators $\mathcal{G}_L : \sigma \mapsto G_L(x, v, v'; \sigma)$ and $\mathcal{G}_R : \sigma \mapsto G_R(x, v, v'; \sigma)$. We fit $\mathcal{G}_L, \mathcal{G}_R$ with DNNs of hidden layer size 128-256-256-128.

Note that, generally, it is not possible to design a DNN taking functions as input. In this work, we consider function $\sigma(x)$ that can be parameterized by a vector \mathbf{p}_σ , that is, a DNN $f_{\theta_L}(x, v, v', \mathbf{p}_\sigma)$ is trained to represent $G_L(x, v, v'; \sigma)$, similarly, another DNN $f_{\theta_R}(x, v, v', \mathbf{p}_\sigma)$ is for $G_R(x, v, v'; \sigma)$.

In Eq. (5.5), when we calculate the 1D integral, similarly we use the Gauss-Legendre integral method. Then we obtain the following representation of MOD-Net solution,

$$u_{\theta_1, \theta_2}(x, v; g_L, g_R, \sigma) = \sum_{v' \in S_{G_v}^+} \omega_{v'_+} f_{\theta_L}(x, v, v'_+, \mathbf{p}_\sigma) g_L(v'_+) + \sum_{v' \in S_{G_v}^-} \omega_{v'_-} f_{\theta_R}(x, v, v'_-, \mathbf{p}_\sigma) g_R(v'_-), \quad (5.6)$$

where $S_{G_v}^+ \subset [0, 1]$, $S_{G_v}^- \subset [-1, 0]$ consist of fixed points determined by Gauss-Legendre integral method and $\omega_{v'_+}, \omega_{v'_-}$ are corresponding coefficients.

5.2 Empirical risk function

For one-dimensional case, to train the neural networks, we would utilize the information of PDE, i.e., governing equation and boundary condition, and a few data $S^{u,k} = \{x_i, v_i, u^k(x_i, v_i)\}_{i \in [n_k]}$ for each $\{g_L^k, g_R^k, \sigma^k\}, k = 1, 2, \dots, K$, where $u^k(\cdot) = u(\cdot; g_L^k, g_R^k, \sigma^k)$. Note that $S^{u,k}$ can be numerically solved by TFMP on coarse grid points, which is not computationally expensive. For each k , we uniformly sample a set of (x, v) from $\Omega \times S = [x_L, x_R] \times [-1, 1]$, i.e., $S^{\Omega, S, k}$ and uniformly sample a set of data from boundaries $\partial\Omega_L = \{(x_L, v)\}_{v \in [0, 1]}$, $\partial\Omega_R = \{(x_R, v)\}_{v \in [-1, 0]}$, respectively, i.e., $S^{\partial\Omega_L, k}, S^{\partial\Omega_R, k}$.

We use the general definition of empirical risk (3.4) for one-dimensional radiative transfer equation. The empirical risk of solving radiative transfer equation is as follows,

$$\begin{aligned}
R_S = & \frac{1}{K} \sum_{k \in [K]} \left(\lambda_1 \frac{1}{|S^{\Omega, S, k}|} \sum_{(x, v) \in S^{\Omega, S, k}} \|v \partial_x u_{\theta_1, \theta_2}(x, v; g_L^k, g_R^k, \sigma^k) + \frac{\sigma_T(x)}{\varepsilon(x)} u_{\theta_1, \theta_2}(x, v; g_L^k, g_R^k, \sigma^k) \right. \\
& - \left(\frac{\sigma_T(x)}{\varepsilon} - \varepsilon \sigma_a(x) \right) \frac{1}{2} \int_{-1}^1 u_{\theta_1, \theta_2}(x, \xi; g_L^k, g_R^k, \sigma^k) d\xi \|_2^2 \\
& + \lambda_{21} \frac{1}{|S^{\partial \Omega_L, k}|} \sum_{(x, v) \in S^{\partial \Omega_L, k}} \|u_{\theta_1, \theta_2}(x, v; g_L^k, g_R^k, \sigma^k) - g_L^k(v)\|_2^2 \\
& + \lambda_{22} \frac{1}{|S^{\partial \Omega_R, k}|} \sum_{(x, v) \in S^{\partial \Omega_R, k}} \|u_{\theta_1, \theta_2}(x, v; g_L^k, g_R^k, \sigma^k) - g_R^k(v)\|_2^2 \\
& \left. + \lambda_3 \frac{1}{|S^{u, k}|} \sum_{i \in [n_k]} \|u_{\theta_1, \theta_2}(x_i, v_i; g_L^k, g_R^k, \sigma^k) - u^k(x_i, v_i)\|_2^2 \right).
\end{aligned}$$

For integral term in the first risk term related to the governing equation of PDE, we use the Gauss-Legendre numerical integral method. We obtain

$$\begin{aligned}
R_S = & \frac{1}{K} \sum_{k \in [K]} \left(\lambda_1 \frac{1}{|S^{\Omega, S, k}|} \sum_{(x, v) \in S^{\Omega, S, k}} \|v \partial_x u_{\theta_1, \theta_2}(x, v; g_L^k, g_R^k, \sigma^k) + \frac{\sigma_T(x)}{\varepsilon(x)} u_{\theta_1, \theta_2}(x, v; g_L^k, g_R^k, \sigma^k) \right. \\
& - \left(\frac{\sigma_T(x)}{\varepsilon} - \varepsilon \sigma_a(x) \right) \frac{1}{2} \sum_{\xi \in S_v} \omega_\xi u_{\theta_1, \theta_2}(x, \xi; g_L^k, g_R^k, \sigma^k) \|_2^2 \\
& + \lambda_{21} \frac{1}{|S^{\partial \Omega_L, k}|} \sum_{(x, v) \in S^{\partial \Omega_L, k}} \|u_{\theta_1, \theta_2}(x, v; g_L^k, g_R^k, \sigma^k) - g_L^k(v)\|_2^2 \\
& + \lambda_{22} \frac{1}{|S^{\partial \Omega_R, k}|} \sum_{(x, v) \in S^{\partial \Omega_R, k}} \|u_{\theta_1, \theta_2}(x, v; g_L^k, g_R^k, \sigma^k) - g_R^k(v)\|_2^2 \\
& \left. + \lambda_3 \frac{1}{|S^{u, k}|} \sum_{i \in [n_k]} \|u_{\theta_1, \theta_2}(x_i, v_i; g_L^k, g_R^k, \sigma^k) - u^k(x_i, v_i)\|_2^2 \right), \tag{5.7}
\end{aligned}$$

where $S_v \subset [-1, 1]$ consists of fixed integration points, determined by Gauss-Legendre integral method and ω_ξ 's are corresponding coefficients.

5.3 Learning process

During training, for each epoch, we first randomly choose $\{(g_L^k, g_R^k, \sigma^k)\}_{k \in [K]}$ and calculate the values of boundary condition g_L^k, g_R^k on fixed integration points $v'_+ \in S_{G_v}^+, v'_- \in S_{G_v}^-$, respectively. Second, we randomly sample points and obtain the data set $S^{\Omega, S, k}, S^{\partial \Omega_L, k}, S^{\partial \Omega_R, k}$. We obtain the data set $D_L = \{(x, v, v'_+, g_L^k(v'_+), \mathbf{p}_\sigma^k) | (x, v) \in S^{\Omega, S, k} \cup S^{\partial \Omega_L, k} \cup S^{\partial \Omega_R, k}, v'_+ \in S_{G_v}^+\}$ and $D_R = \{(x, v, v'_-, g_R^k(v'_-), \mathbf{p}_\sigma^k) | (x, v) \in S^{\Omega, S, k} \cup S^{\partial \Omega_L, k} \cup S^{\partial \Omega_R, k}, v'_- \in S_{G_v}^-\}$. In the following, for

each k , we feed the data D_L, D_R into the neural network $f_{\theta_L}(x, v, v', \mathbf{p}_\sigma), f_{\theta_R}(x, v, v', \mathbf{p}_\sigma)$ respectively, and calculate the empirical risk (5.7) defined utilizing the governing equation of PDE, boundary condition and a few labeled data $S^{u,k}$. We train neural network f_{θ_L} and f_{θ_R} with Adam to minimize the empirical risk, and finally obtain well-trained green's function DNNs f_{θ_L} and f_{θ_R} , furthermore, according to (5.6), we obtain a neural operator $u_{\theta_1, \theta_2}(x, v; g_L, g_R, \sigma)$.

5.4 Results

For convenience, we fixed the $\sigma = (\sigma_T, \sigma_a, \varepsilon)$, only learn a operator mapping from g_L, g_R to the solution u of the radiative transfer equation. To see the performance of obtained operator, we need the reference solution. Since it is difficult to obtain the analytical solution of radiative transfer equation, we use the TFMP method to obtain the numerical solution as reference.

5.4.1 Example 3: Radiative transfer equation of the first type of σ

We initially consider a simple case, $x_L = 0, x_R = 2$ and $\sigma_T(x) = 5, \sigma_a(x) = 1$. To avoid the multi-scale phenomenon, we take $\varepsilon(x) = 1$. For generality, we set the boundary condition $g_L = g_R = a_1 \cos(\omega x) + a_2 \sin(\omega x) + 2$, which is determined by a_1, a_2, ω . In fact, many boundary conditions can be represented with these basic functions. And for convenience, we set $\omega = 1, a_2 = 1$ and only change a_1 . Then the boundary condition is $g_L = g_R = a_1 \cos(x) + \sin(x) + 2$. Note that for this type of σ , we need no labeled data, i.e., in (5.7), $\lambda_3 = 0$.

To solve the PDE with various a_1 accurately and quickly, we use MOD-Net approach to train a neural operator. We set $K = 20$ and for each epoch, we sample K boundary conditions through sampling a_1 . Here for simplicity, we sample control parameter a_1 uniformly from $\{0.03k\}_{k=1}^{33}$.

In training, we set the number of integration points $|S_{G_v}^+| = 30, |S_{G_v}^-| = 30, |S_v| = 30$, and for each epoch, for each k , we uniformly sample 500 points in $[0, 2] \times [-1, 1]$ for $S^{\Omega, S, k}$, 500 points v_i 's in $[0, 1]$ for $S^{\partial\Omega_L, k} = \{(0, v_i) | i = 1, \dots, 500\}$, another 500 points v_i 's in $[-1, 0]$ for $S^{\partial\Omega_R, k} = \{(2, v_i) | i = 1, \dots, 500\}$. The empirical risk, i.e., training loss is shown in Fig. 5. The total training loss (indicated by blue curve) decays with training epoch. For visualization of each part of the total training loss, we also display the residual loss of the radiative transfer equation (indicated by orange curve) and the loss of two boundary lines (other two colored curves), which decay with the training epoch except that slight oscillation appears in the final stage.

To test the performance of the trained MOD-Net on $a_1 = 0.02, 0.11, 0.51, 0.99$, we calculate the density function $\rho(x)$ of u , i.e., $\rho(x) = \frac{1}{2} \int_{-1}^1 u(x, \xi) d\xi$, by Gaussian-Legendre integral method, and obtain $\rho(x) = \frac{1}{2} \sum_{\xi \in S_v} \omega_\xi u(x, \xi)$, where $S_v \subset [-1, 1]$ consists of the Gaussian-Legendre integral points and ω_ξ 's are corresponding coefficients. For various a_1 , the density function of MOD-Net solution and numerical solution by TFMP method with isometric grids $(x_i, v_j)_{i \in [101], j \in [60]}$ are very consistent as shown in Fig. 6. For visualization,

we also plot the MOD-Net solution and the corresponding numerical solution on $x=0,1,2$ for various test a_1 . As shown in Fig. 7, the MOD-Net solutions overlap well with the numerical solutions for various test a_1 , except a little shift on the left boundary.

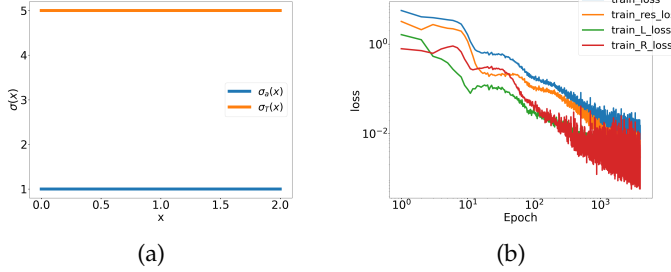


Figure 5: Example 3. (a) $\sigma_T(x)$ and $\sigma_a(x)$ vs. x . (b) Training loss vs. for the learning of the operator of radiative transfer equation with constant $\sigma_T(x)$, $\sigma_a(x)$. The blue curve is the total risk Eq. (5.7). The other three curves represent three terms in the total risk Eq. (5.7) except the last term, respectively.

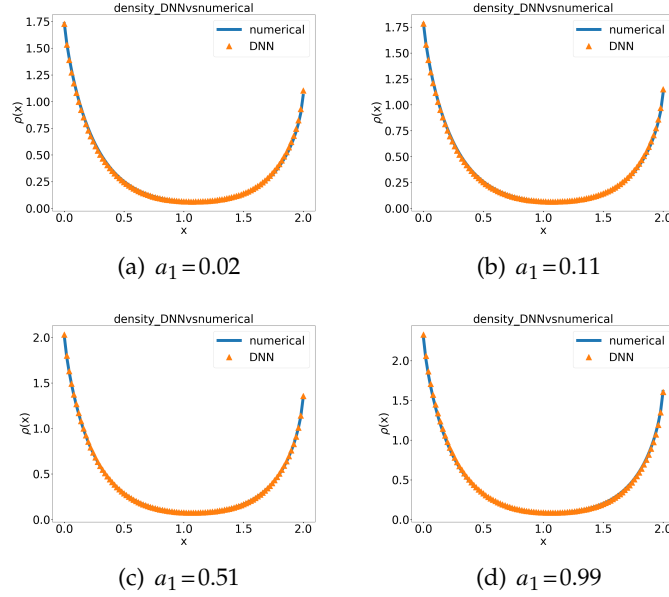


Figure 6: Example 3. Comparison between numerical solution and MOD-Net solution on density function corresponding to each of four boundary conditions $g_L = g_R = a_1 \cos(x) + \sin(x) + 2$ determined by $a_1 = 0.02, 0.11, 0.51, 0.99$.

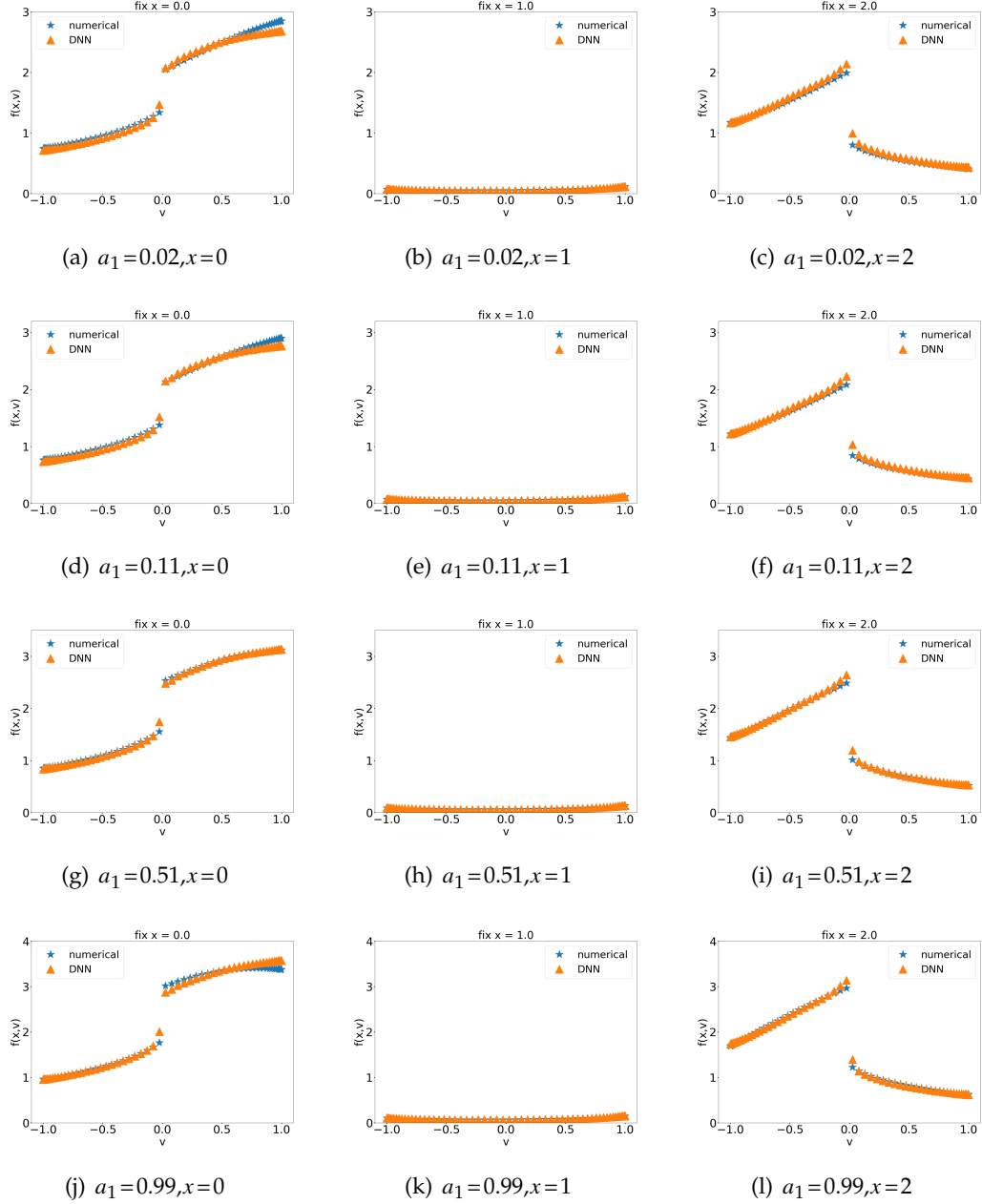


Figure 7: Example 3. Comparison between numerical solution and MOD-Net solution on $x=0,1,2$ corresponding to each of four boundary conditions $g_L=g_R=a_1 \cos(x)+\sin(x)+2$ determined by $a_1=0.02,0.11,0.51,0.99$.

5.4.2 Radiative transfer equation of Second type σ

Then we consider $\sigma_T(x)=5$ and $\sigma_a(x)$ are varying with x rather than constant. We set

$$\sigma_T(x)=\begin{cases} x+1, & 0 \leq x < 1, \\ 2, & 1 \leq x \leq 2, \end{cases} \quad (5.8)$$

and

$$\sigma_a(x)=\begin{cases} x, & 0 \leq x < 1, \\ 1, & 1 \leq x \leq 2, \end{cases} \quad (5.9)$$

the graphs of which are shown in Fig. 8(a). For convenience, we set the boundary condition $g_L=g_R=\cos(x)+a_2\sin(x)+2$. For this case, if we train MOD-Net with only the PDE, i.e., governing equation and boundary condition, or only the a few labeled data, the performance is not satisfying.

Example 4. Neural solver for one radiative transfer equation Fix $a_2=0.01$, by TFPM method, we obtain 20 labeled data on coarse grids, i.e., 5 discrete points in x direction and 4 discrete points in v direction.

We train the solver of the radiative transfer equation with three different loss functions. First, we set the λ_3 in (5.7) be zero, i.e., training the MOD-Net only by the governing equation and boundary conditions, the empirical risk, i.e., training loss is shown in Fig. 8(b). To test the performance of the obtained MOD-Net solution u , we calculate the density function $\rho(x)$ of u . The density function of the MOD-Net solution and numerical TFMP solution with isometric grids $(x_i, v_j)_{i \in [101], j \in [60]}$ are significantly different, as shown in Fig. 8(c). For visualization, we plot the MOD-Net solution and the corresponding numerical solution on $x=0,1,2$. As shown in Fig. 8(d, e, f), the MOD-Net solution is far from the numerical solution.

Second, $\lambda_1, \lambda_{21}, \lambda_{22}$ in (5.7) are set as zero, i.e., training the MOD-Net by only the 20 labeled data with the training loss shown in Fig. 9(b). The training loss (indicated by blue curve) decays with training epoch except oscillation appears in the final stage. We use the trick of early stopping with tolerance 50 to obtain a DNN with small loss. Similarly, to test the performance of the obtained MOD-Net solution u , we calculate the density function $\rho(x)$ of u . The density function of the MOD-Net solution and TFMP solution have clear difference as shown in Fig. 9(c). For visualization, we plot the MOD-Net solution and the corresponding numerical solution on $x=0,1,2$. As shown in Fig. 9(d, e, f), the MOD-Net solution significantly deviates from the numerical solution.

Finally, we train the MOD-Net by the governing equation, boundary condition and 20 labeled data simultaneously, the training loss decays with training epoch as shown in Fig. 10(b). Similarly, we calculate the density function of MOD-Net solution and TFMP solution. They are very consistent as shown in Fig. 10(c). As shown in Fig. 10(d, e, f), the MOD-Net solution overlap well with the numerical solution very well except for the discontinuous points.

To sum up, with the information of only PDE or only a few labeled data, the MOD-Net cannot be trained well, however, combining these two information, we can train the MOD-Net very well.

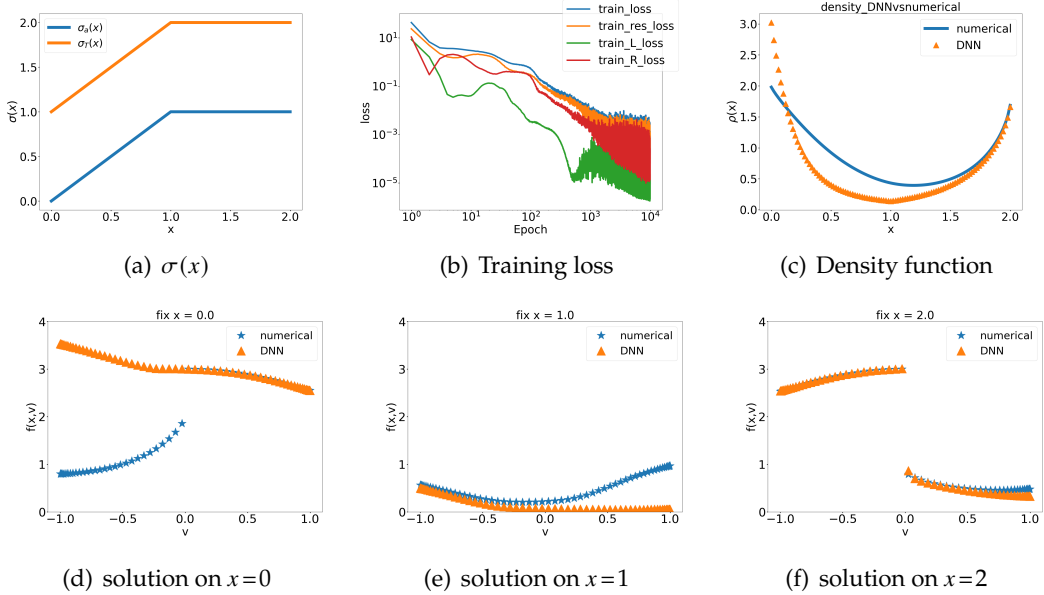


Figure 8: Example 4. Trained by only the PDE, i.e., the governing equation and boundary condition. (a) The graphs of $\sigma_T(x)$ and $\sigma_a(x)$ in considered radiative transfer equation. (b) Training loss. The blue curve is the total risk Eq. (5.7). The other three curves represent three terms in the total risk Eq. (5.7) except the last term, respectively. (c) Comparison between numerical solution and MOD-Net solution on density function. (d, e, f) Comparison between numerical solution and MOD-Net solution on $x=0, 1, 2$.

Example 5: MOD-Net for radiative transfer equation To solve the PDE with various a_2 accurately and quickly, we use MOD-Net approach to learn a neural operator.

We set $K=20$ and for each epoch, we sample K a_2 's uniformly from $\{0.03k\}_{k=1}^{33}$. In training, we set the number of integration points $|S_{G_v}^+|=30, |S_{G_v}^-|=30, |S_v|=30$, and for each epoch, for each k , similarly, we uniformly sample 500 points in $[0,2] \times [-1,1]$ for $S^{\Omega, S, k}$, 500 points v_i 's in $[0,1]$ for $S^{\partial\Omega_L, k} = \{(0, v_i) | i=1, \dots, 500\}$, another 500 points v_i 's in $[-1,0]$ for $S^{\partial\Omega_R, k} = \{(2, v_i) | i=1, \dots, 500\}$. The training loss is shown in Fig. 11(b). The total risk (indicated by blue curve) decays with training epoch. For visualization of each part of the total risk, we also display the residual loss of the radiative transfer equation (indicated by orange curve), the loss of two boundary lines (indicated by green and red curves) and the loss of supervised data (indicated by remaining curve), which decay with the training epoch overall.

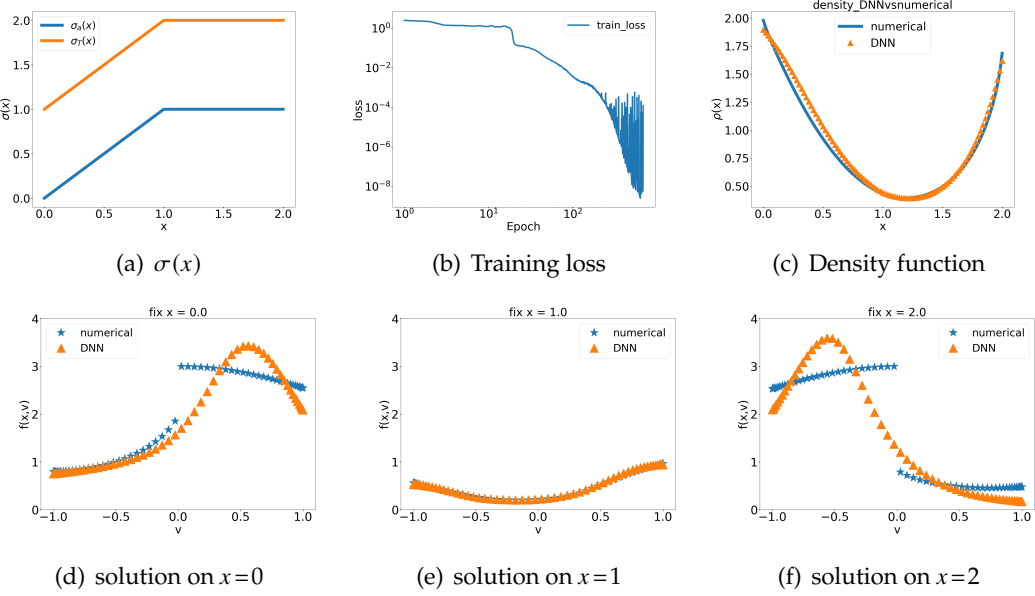


Figure 9: Example 4. Trained by only the labeled data. (a) The graphs of $\sigma_T(x)$ and $\sigma_a(x)$ in considered radiative transfer equation. (b) Training loss. The blue curve is the last term in total risk Eq. (5.7). (c) Comparison between numerical solution and MOD-Net solution on density function. (d, e, f) Comparison between numerical solution and MOD-Net solution on $x=0,1,2$.

To test the performance of the trained MOD-Net on $a_2=0.02, 0.11, 0.51, 0.99$. Similarly, for each a_2 , we calculate the density function $\rho(x)$ of the solution. For all a_2 's, the density function of MOD-Net solution and numerical solution by TFMP method with isometric grids $(x_i, v_j)_{i \in [101], j \in [60]}$ are very consistent as shown in Fig. 12. For visualization, we also plot the MOD-Net solution and the corresponding numerical solution on $x=0,1,2$. As shown in Fig. 13, the MOD-Net solutions overlap well with the numerical solutions for all cases.

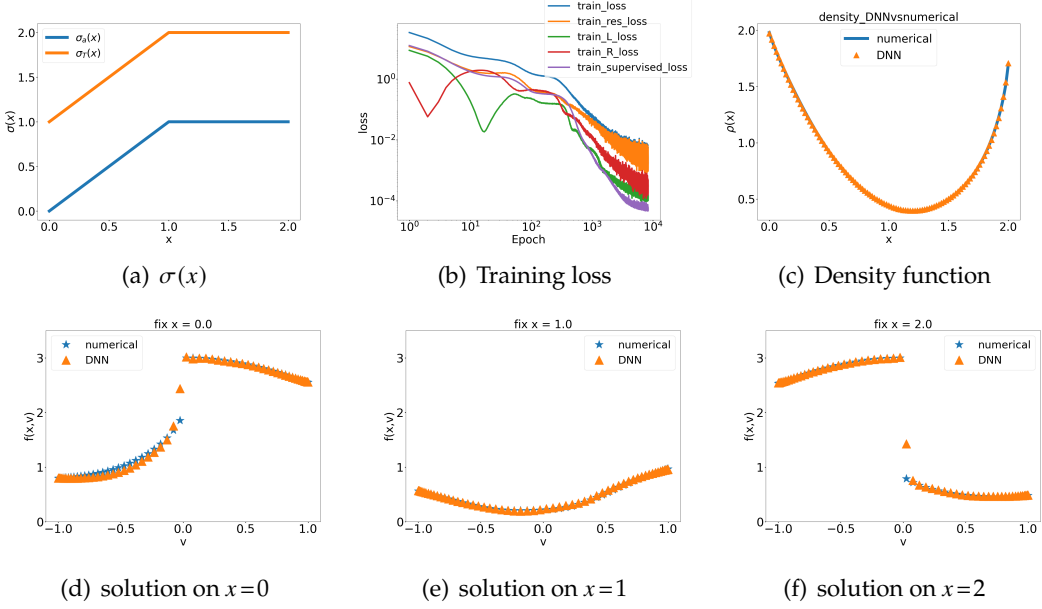


Figure 10: Example 4. Trained by the governing PDE, boundary condition, and coarse grid data together. (a) The graphs of $\sigma_T(x)$ and $\sigma_a(x)$ in considered radiative transfer equation. (b) Training loss. The blue curve is the total risk Eq. (5.7). The other four curves represent four terms in the total risk Eq. (5.7), respectively. (c) Comparison between numerical solution and MOD-Net solution on density function. (d, e, f) Comparison between numerical solution and MOD-Net solution on $x=0,1,2$.

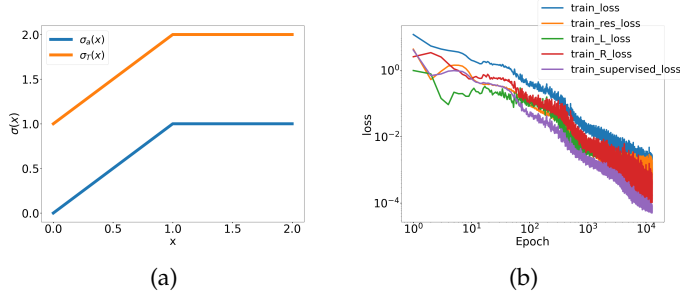


Figure 11: Example 5. (a) $\sigma_T(x)$ and $\sigma_a(x)$ vs. x . (b) Training loss vs. epoch for the learning of the operator of radiative transfer equation with continuous $\sigma_T(x)$, $\sigma_a(x)$. The blue curve is the total risk Eq. (5.7). The other four curves represent four terms in the total risk Eq. (5.7), respectively.

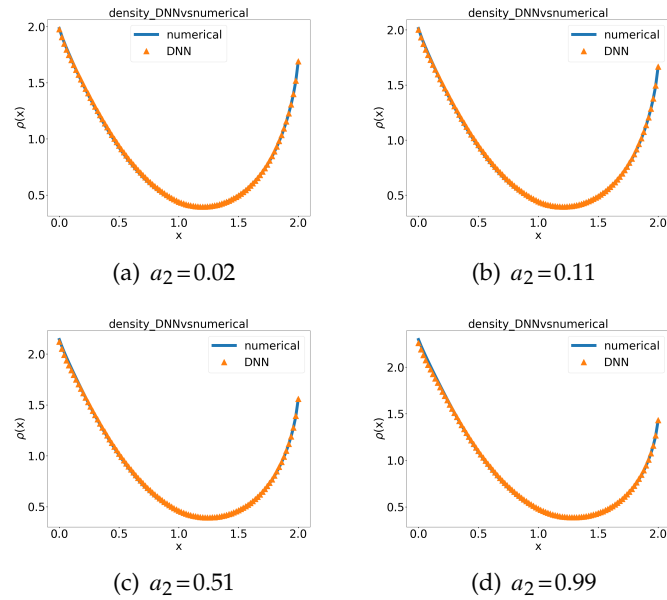


Figure 12: Example 5. Comparison between numerical solution and MOD-Net solution on density function corresponding to each of four boundary conditions $g_L = g_R = \cos(x) + a_2 \sin(x) + 2$ determined by $a_2 = 0.02, 0.11, 0.51, 0.99$.

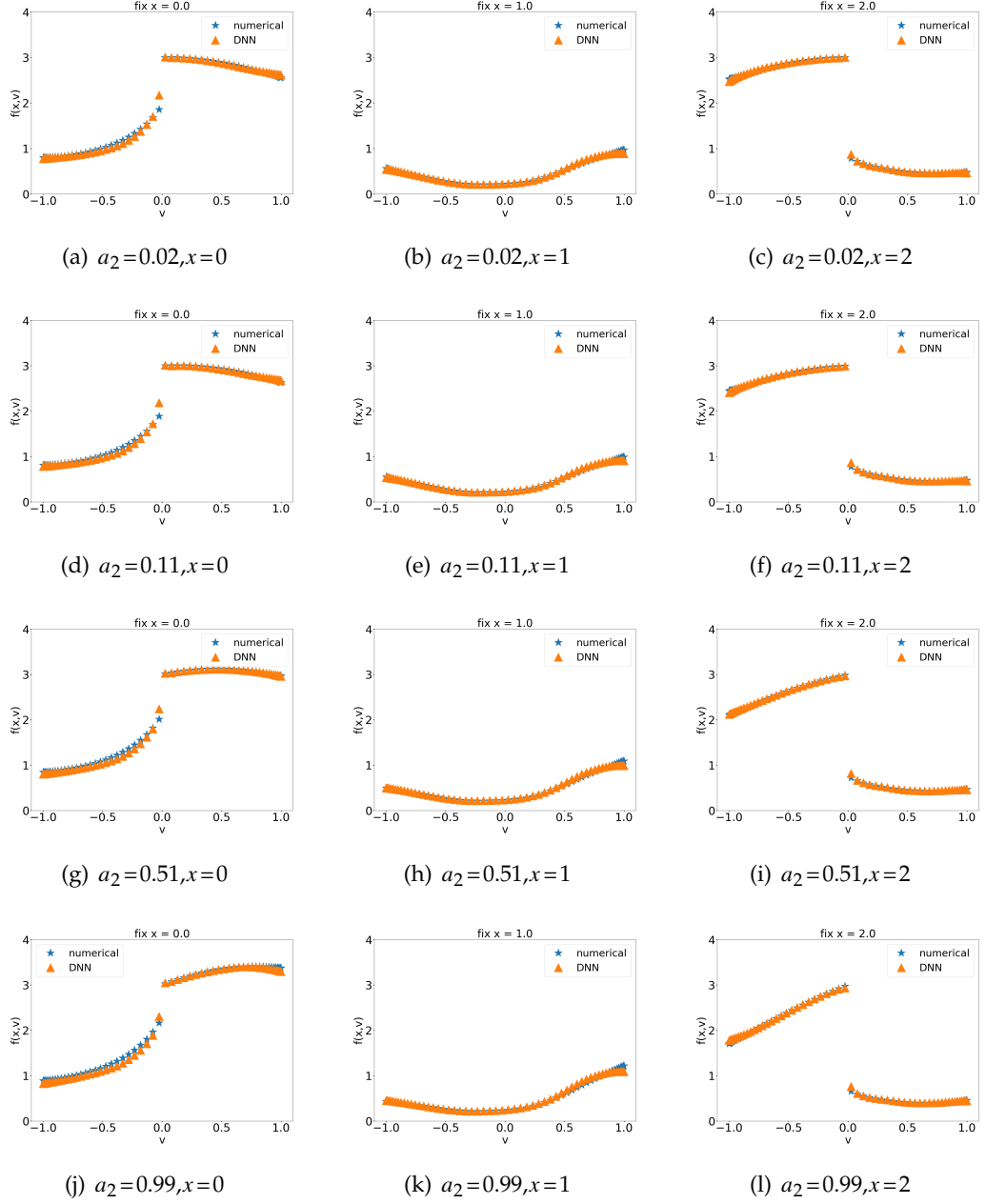


Figure 13: Example 5. Comparison between numerical solution and MOD-Net solution on $x=0,1,2$ corresponding to each of boundary conditions $g_L=g_R=\cos(x)+a_2\sin(x)+2$ determined by $a_2=0.02,0.11,0.51,0.99$.

6 Conclusion

In this work, we propose a model-operator-data network (MOD-Net) for solving PDEs. For simple problems, the empirical risk of MOD-Net only requires the physical information of the PDE and does not require any labeled data. For difficult problems, such as the problems of discontinuous solutions, we show that the MOD-Net can be well trained with the regularization of a few labeled data, which are computed by traditional numerical schemes on the coarse grid points with cheap computational cost. The great advantage of the MOD-Net is that it solves a type of PDEs but not a specific one in a meshless way without expensive labeled data.

In the future works, we would apply MOD-Net approach to high-dimensional problems and inverse problems. The current MOD-Net approach applies to linear PDE, while with slight modification, similar non-linear MOD-Net approach can be estimated.

Acknowledgments

This work is sponsored by the National Key R&D Program of China Grant No. 2019YFA0709503 (Z. X.), the Shanghai Sailing Program, the Natural Science Foundation of Shanghai Grant No. 20ZR1429000 (Z. X.), the National Natural Science Foundation of China Grant No. 62002221 (Z. X.), Shanghai Municipal of Science and Technology Project Grant No. 20JC1419500 (Y.Z.), the National Natural Science Foundation of China Grant No. 12031013 (Z. M.), Shanghai Municipal of Science and Technology Major Project No. 2021SHZDZX0102, and the HPC of School of Mathematical Sciences and the Student Innovation Center at Shanghai Jiao Tong University.

References

- [1] Wei Cai, Xiaoguang Li, and Lizuo Liu. A phase shift deep neural network for high frequency approximation and wave problems. *SIAM Journal on Scientific Computing*, 42(5):A3285–A3312, 2020.
- [2] Subrahmanyam Chandrasekhar. *Radiative transfer*. Courier Corporation, 2013.
- [3] Weinan E, Jiequn Han, and Arnulf Jentzen. Deep learning-based numerical methods for high-dimensional parabolic partial differential equations and backward stochastic differential equations. *Communications in Mathematics and Statistics*, 5(4):349–380, 2017.
- [4] Weinan E and Bing Yu. The deep ritz method: A deep learning-based numerical algorithm for solving variational problems. *Communications in Mathematics and Statistics*, 6(1):1–12, 2018.
- [5] Yuwei Fan, Lin Lin, Lexing Ying, and Leonardo Zepeda-Núñez. A multiscale neural network based on hierarchical matrices. *Multiscale Modeling & Simulation*, 17(4):1189–1213, 2019.
- [6] A Hamilton, T Tran, MB Mckay, B Quiring, and PS Vassilevski. Dnn approximation of nonlinear finite element equations. Technical report, Lawrence Livermore National Lab.(LLNL), Livermore, CA (United States), 2019.
- [7] Juncai He, Lin Li, Jinchao Xu, and Chunyue Zheng. Relu deep neural networks and linear finite elements. *Journal of Computational Mathematics*, 38(3):502–527, 2020.

- [8] Shi Jin, Min Tang, and Houde Han. A uniformly second order numerical method for the one-dimensional discrete-ordinate transport equation and its diffusion limit with interface. *Networks & Heterogeneous Media*, 4(1):35, 2009.
- [9] Jacqueline Lenoble. *Radiative transfer in scattering and absorbing atmospheres: standard computational procedures*, volume 300. A. Deepak Hampton, Va., 1985.
- [10] Xi-An Li, Zhi-Qin John Xu, and Lei Zhang. A multi-scale dnn algorithm for nonlinear elliptic equations with multiple scales. *Communications in Computational Physics*, 28(5):1886–1906, 2020.
- [11] Zongyi Li, Nikola Kovachki, Kamyar Azizzadenesheli, Burigede Liu, Kaushik Bhattacharya, Andrew Stuart, and Anima Anandkumar. Fourier neural operator for parametric partial differential equations. *arXiv preprint arXiv:2010.08895*, 2020.
- [12] Zongyi Li, Nikola Kovachki, Kamyar Azizzadenesheli, Burigede Liu, Kaushik Bhattacharya, Andrew Stuart, and Anima Anandkumar. Neural operator: Graph kernel network for partial differential equations. *arXiv preprint arXiv:2003.03485*, 2020.
- [13] Yulei Liao and Pingbing Ming. Deep nitsche method: Deep ritz method with essential boundary conditions. *Communications in Computational Physics*, 29(5):1365–1384, 2021.
- [14] Ziqi Liu, Wei Cai, and Zhi-Qin John Xu. Multi-scale deep neural network (mscalednn) for solving poisson-boltzmann equation in complex domains. *Communications in Computational Physics*, 28(5):1970–2001, 2020.
- [15] Stefano Markidis. Physics-informed deep-learning for scientific computing. *arXiv preprint arXiv:2103.09655*, 2021.
- [16] Maziar Raissi, Paris Perdikaris, and George E Karniadakis. Physics-informed neural networks: A deep learning framework for solving forward and inverse problems involving nonlinear partial differential equations. *Journal of Computational Physics*, 378:686–707, 2019.
- [17] Carlos Michelen Strofer, Jin-Long Wu, Heng Xiao, and Eric Paterson. Data-driven, physics-based feature extraction from fluid flow fields using convolutional neural networks. *Communications in Computational Physics*, 25(3):625–650, 2019.
- [18] Matthew Tancik, Pratul P. Srinivasan, Ben Mildenhall, Sara Fridovich-Keil, Nithin Raghavan, Utkarsh Singhal, Ravi Ramamoorthi, Jonathan T. Barron, and Ren Ng. Fourier features let networks learn high frequency functions in low dimensional domains. *arXiv preprint arXiv:2006.10739*, 2020.
- [19] Sifan Wang, Hanwen Wang, and Paris Perdikaris. On the eigenvector bias of Fourier feature networks: From regression to solving multi-scale PDEs with physics-informed neural networks. *Computer Methods in Applied Mechanics and Engineering*, 384(C), 2021.
- [20] Zhi-Qin John Xu, Yaoyu Zhang, Tao Luo, Yanyang Xiao, and Zheng Ma. Frequency principle: Fourier analysis sheds light on deep neural networks. *Communications in Computational Physics*, 28(5):1746–1767, 2020.
- [21] Zhi-Qin John Xu, Yaoyu Zhang, and Yanyang Xiao. Training Behavior of Deep Neural Network in Frequency Domain. In *Neural Information Processing*, Lecture Notes in Computer Science, pages 264–274, 2019.